account for the large magnitude of the acoustic signal seen in the cylindrical excitation geometry, the audible sound, and the failure of both of these signals to disappear at low temperature. The reaction of carbon with water takes place at temperatures on the order of hundreds of degrees Celsius; thus, the production and expansion of gas should be essentially independent of temperature for a change as small as 10°C. The induction period for the photoacoustic effect in carbon suspensions can, in all likelihood, be ascribed either to the increased reactivity of the new, large-diameter particles that are formed during irradiation or to the development of reaction centers in the graphitic component of the carbon, as has been noted for the steam-carbon reaction (*23*).

The theory given here for chemical generation of the photoacoustic effect should be rigorously correct for differential changes in the state variables. However, its application to the present rather complicated problem, where high-temperature reactions and gas expansion are involved, is speculative. In addition to chemical reaction, phenomena such as temperature-dependent thermal expansion (*1*, *5*, *24*), nonlinear heat conduction (*25*), vaporization of fluid around the perimeter of the particle (*20*), and even shock-wave formation are possibly involved in the generation of the photoacoustic effect. The unusual properties of the photoacoustic effect in carbon suspensions, its ease of production (*26*), and its dependence on chemical reaction argue for more experimentation and, most certainly, for formulation of a more sophisticated theoretical model for sound wave generation.

REFERENCES AND NOTES

1. V. E. Gusev and A. A. Karabutov, *Lazernaya Optoakustika* (Naoka, Moscow, 1991) [transl., *Laser Optoacoustics* (AIP Press, New York, 1993)].
2. F. V. Bunkin, Al A. Kolomensky, V. G. Mikhalevich, *Lasers in Acoustics* (Harwood Academic, Reading, MA, 1991).
3. S. V. Egerev, L. M. Lyamshev, O. V. Puchenkov, *Usp. Fiz. Nauk* **160**, 111 (1990) [*Sov. Phys. Usp.* **33**, 739 (1990)].
4. S. A. Akhmanov, V. E. Gusev, A. A. Karabutov, *Infrared Phys.* **29**, 815 (1989).
5. A. C. Tam, *Rev. Mod. Phys.* **58**, 381 (1986).
6. A. I. Bozhkov, F. V. Bunkin, Al. A. Kolomenskii, V. G. Mikhalevich, *Sov. Sci. Rev.* **3**, 459 (1981).
7. C. K. N. Patel and A. C. Tam, *Rev. Mod. Phys.* **53**, 517 (1981).
8. L. M. Lyamshev, *Usp. Fiz. Nauk* **135**, 637 (1981) [*Sov. Phys. Usp.* **24**, 977 (1981)].
9. Experiments were done with "Black Pearls 470" (Cabot Inc.). The diameters of the individual particles were determined from electron micrographs to be on the order of 30 nm. The agglomeration seen on the micrographs was consistent with the 94-nm hydrodynamic diameter specified by the manufacturer.
10. G. J. Diebold, M. I. Khan, S. M. Park, *Science* **250**, 101 (1990).
11. M. I. Khan, T. Sun, G. J. Diebold, *J. Acoust. Soc. Am.* **94**, 931 (1993).
12. G. J. Diebold, T. Sun, M. I. Khan, *Phys. Rev. Lett.* **67**, 3384 (1991).
13. A number of experiments were done with different carbon and dye solutions. The suspension with the largest normalized experiment had an undiluted absorption coefficient of $\bar{\alpha} = 0.092\ cm^{-1}$. This solution was diluted by a factor of 500 in the photoacoustic cell and gave a photoacoustic signal of 150 mV. The malachite green dye solution used for comparison had $\bar{\alpha} = 0.07\ cm^{-1}$ and gave a photoacoustic signal of 20 mV.
14. H. J. Eichler, P. Gunter, D. W. Pohl, *Laser-Induced Dynamic Gratings* (Springer-Verlag, Berlin, 1985).
15. R. J. D. Miller, in *Time Resolved Spectroscopy*, R. J. H. Clark and R. E. Hester, Eds. (Wiley, New York, 1989), pp. 1–54.
16. M. D. Fayer, *IEEE J. Quantum Electron.* **QE-22**, 1437 (1986).
17. A. R. Duggal and K. A. Nelson, *J. Chem. Phys.* **94**, 7677 (1991).
18. Purchased from Ted Pella, Inc. The diameter of the gold particles is specified to be 40 nm with a standard deviation of ±10 nm, at a concentration of 5.8×10^{-2} g liter^{-1} or 9×10^{10} particles per milliliter.
19. J. Morais, J. Ma, M. B. Zimmt, *J. Phys. Chem.* **95**, 3885 (1991).
20. The production of gas is corroborated by the work of K. J. McEwan and P. A. Madden [*J. Chem. Phys.* **97**, 8748 (1992)], who inferred the production of bubbles around the particles by carrying out experiments with pressurized carbon suspensions. H. Lowne and P. A. Madden [*J. Chem. Phys.* **97**, 8760 (1992)] gave a model for sound production based on fluid vaporization.
21. P. Morse and K. U. Ingard, *Theoretical Acoustics* (Princeton Univ. Press, Princeton, NJ, 1968).
22. The chemical expansion coefficient β_c given here should be the molar volume change determined experimentally by a number of organic photochemists and discussed by S. E. Braslavsky and H. E. Heibel [*Chem. Rev.* **92**, 1381 (1992)]; both have the same dimensions. Note that Eq. 5 has been calculated to zeroth order in $\hat{\ell}_h$ in the acoustic mode. The effects of viscosity have not been included in the abbreviated solution given here. For a complete solution, see H. Chen and G. Diebold (in preparation).
23. C. G. von Fredersdorff and M. A. Elliott, in *The Chemistry of Coal Utilization*, Supplementary Volume, H. H. Lowry, Ed. (Wiley, New York, 1963), pp. 918–925. In the limit where the particle diameter is much smaller than the wavelength of the optical radiation, it is easy to show that the final temperature of a particle is independent of its radius if there are no thermal loss mechanisms. When heat is lost from a particle by thermal conduction, calculations show that large particles remain at an elevated temperature longer than small ones, indicating a higher effective reactivity for large particles.
24. M. W. Sigrist, *J. Appl. Phys.* **60**, R83 (1986).
25. V. Gusev, A. Mandelis, R. Bleiss, *Int. J. Thermophys.* **14**, 321 (1993).
26. A. Harata and T. Sawada (in preparation) have found large signals and nonlinear effects from carbon suspensions in experiments with surface waves on fluids.

27. This research was supported by the U.S. Department of Energy, Office of Basic Energy Studies, under grant ER-13235.

26 May 1995; accepted 12 September 1995

Supramolecular Second-Order Nonlinearity of Polymers with Orientationally Correlated Chromophores

Martti Kauranen, Thierry Verbiest, Carlo Boutton, M. N. Teerenstra, Koen Clays, A. J. Schouten, R. J. M. Nolte, André Persoons*

Nonlinear optical chromophores can be organized as orientationally correlated side groups of polymers with a rigid backbone. In such an organization, each chromophore contributes coherently to the second-order nonlinear response of the polymer structure. A first hyperpolarizability exceeding 5000×10^{-30} electrostatic units was measured for a poly(isocyanide) structure containing ~100 chromophores by means of hyper-Rayleigh scattering. Electric field–induced second-harmonic generation measurements confirmed that the product of the permanent dipole moment and the first hyperpolarizability was enhanced for the polymer structure. These results provide guidelines for future efforts to optimize supramolecular structures for applications in second-order nonlinear optics.

Organic molecules are widely regarded as one of the most promising groups of materials for applications in nonlinear optics (*1*). For several important applications, such as electro-optic modulation or frequency doubling, materials with second-order nonlinearity are required. Only noncentrosymmetric molecules (or aggregates) can possess a second-order nonlinear response, that is, a nonvanishing first molecular hyperpolarizability. Moreover, the molecules cannot be useful in devices unless they are incorporated into a noncentrosymmetric macroscopic structure, which has a nonvanishing second-order susceptibility. The achievement of such macroscopic ordering is a formidable task, because the permanent dipole moments of noncentrosymmetric molecules tend to pair in opposite directions to give rise to a centrosymmetric macroscopic structure.

The most common way to break the

M. Kauranen, T. Verbiest, C. Boutton, K. Clays, A. Persoons, Laboratory of Chemical and Biological Dynamics and Center for Research on Molecular Electronics and Photonics, University of Leuven, B-3001 Heverlee, Belgium.

M. N. Teerenstra and A. J. Schouten, Laboratory of Polymer Science, University of Groningen, 9747 AG Groningen, Netherlands.

R. J. M. Nolte, Department of Organic Chemistry, University of Nijmegen, 6525 ED Nijmegen, Netherlands.

*To whom correspondence should be addressed.

centrosymmetry is through poling with a static electric field (*1*); the degree of ordering that can be achieved through poling depends linearly on both the permanent dipole moment of the molecules and the poling field. Alternatively, second-order nonlinear devices can be constructed by organizing the nonlinear molecules as chromophores into a noncentrosymmetric supramolecular structure (*2*). When such structures extend to macroscopic dimensions, the poling of the chromophores can be achieved through chemical synthesis, with no need for external poling. For microscopic (smaller than wavelength) structures, the nonlinearity can be discussed in terms of a supramolecular hyperpolarizability (*3*), which grows linearly as a function of the number of orientationally correlated chromophores. The permanent dipole moment of such a structure can be very large, either because of the coherent addition of the dipole moments of the chromophores (*4*) or because of the dipole moment associated with the supramolecular structure itself (*5*). The degree of alignment of supramolecular units that can be achieved for a given strength of the poling field would then be greater than that of the individual chromophores. Here, we show that nonlinear optical chromophores can be organized in a fixed noncentrosymmetric arrangement as side groups of polymers with a rigid backbone, and we present experimental evidence of the large second-order nonlinearity of the supramolecular structure.

We have investigated the second-order response of poly(isocyanide)s (*6*) that contain nonlinear chromophores as side groups (Fig. 1) (*7*). The key property of poly(isocyanide)s with bulky side groups is the rigid and extended helical chain conformation of the backbone (*6*, *8*), which results in a strong orientational correlation of the side groups (Fig. 2). The chromophores were chosen for the well-known nonlinear properties of donor-acceptor–functionalized azobenzenes (*1*). In the samples investigated, a total of ~100 chromophores (~25 helical turns, ~3.8 chromophores per turn) are stacked in four twisted columns over the length (~10 nm) of the polymer. There is no net alignment of chromophores in the transverse direction. However, the centrosymmetry of the structure is broken in the direction of the axis of the helical backbone, because all chromophores form an equal angle with respect to this axis. This angle is ~60°, as estimated by molecular mechanics calculations using the consistent force field method (*9*).

The rigid conformation of poly(isocyanide)s is also stable in solution, and we have determined the first hyperpolarizability of the compounds in Fig. 1 by hyper-Rayleigh scattering (HRS) (*10*–*12*) with chloroform as the solvent. HRS is a nonlinear light-scattering process in which two incident photons at the fundamental frequency ω give rise to a scattered photon at the second-harmonic frequency 2ω. In our experiments (Fig. 3), these frequencies correspond to wavelengths of 1064 and 532 nm, respectively. Our compounds exhibited no fluorescence at 532 nm that could hamper the HRS measurements. The principal absorption band of the compounds peaks between 400 and 500 nm (Table 1) and extends to 532 nm. Hence, the second-harmonic generation process is enhanced by a two-photon resonance of the fundamental wavelength. Note also that the absorption bands of the polymers are blue-shifted with respect to those of the chromophores. The intensity of the scattered second-harmonic light is of the form

$$I_{2\omega} = gB^2I_\omega^2 \quad (1)$$

(*11*), where I_ω is the intensity of the fundamental beam and g is an instrumental factor that accounts for the scattering geometry and the local field factors. The effective nonlinearity B of the solution is

$$B^2 = N_{solvent}\beta^2_{solvent} + N_{solute}\beta^2_{solute} \quad (2)$$

where N is the number density and β is the hyperpolarizability. In our experimental procedure, we measured the quadratic coefficient gB^2 as a function of the number density of the solute. This function yields the hyperpolarizability of the solute after an exponential loss factor is applied that accounts for the absorption of the second-harmonic light (*12*). *p*-Nitroaniline ($\beta = 23 \times 10^{-30}$ esu) was used as the reference (*11*).

The hyperpolarizabilities of the polymer compounds were much larger than those of the respective chromophores (Table 1). This finding indicates that the chromophores are organized in a noncentrosymmetric arrangement in the polymer chain and that each chromophore contributes coherently to the hyperpolarizability of the polymer. The hyperpolarizabilities of the polymers are very large, even for resonantly enhanced values. The rigidity of the polymers is essential to this observed increase in hyperpolarizability; in earlier work, the hyperpolarizability of chromophores incorporated into a polymer with a flexible backbone was found to be independent of the polymeric environment (*13*).

To determine how well the measured hyperpolarizabilities of the polymers could be explained by those of the chromophores, we assumed that the hyperpolarizability of the polymers can be calculated by summing over the contributions of each chro-

1a

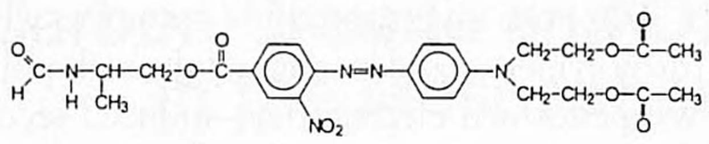

1b

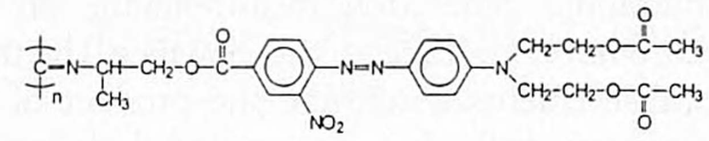

2a

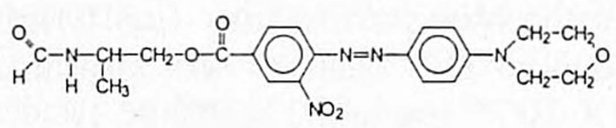

2b

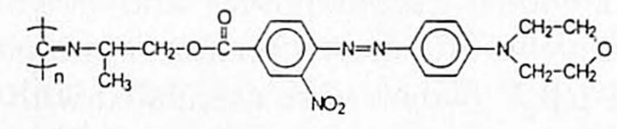

Fig. 1. Chemical structures of the chromophores (**1a** and **2a**) and the poly(isocyanide)s (**1b** and **2b**). Polymers **1b** and **2b** were synthesized from (*S*)- and (*R,S*)-isocyanide monomers, respectively (*17*).

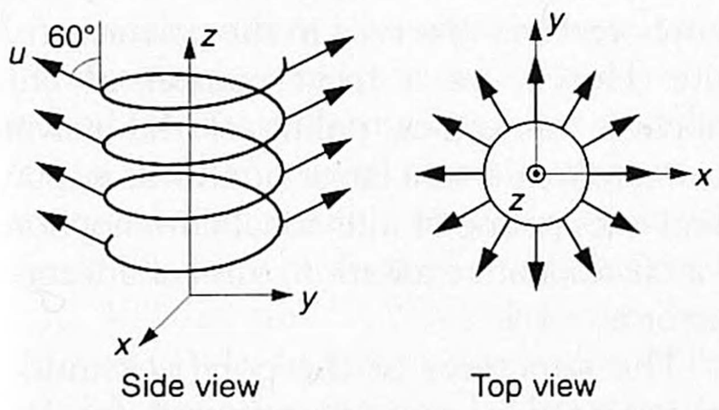

Fig. 2. Helical structure of poly(isocyanide)s with nonlinear optical chromophores. The coordinate system *uvw*, with the *u* axis along the long axis of the chromophores, defines the frame of reference for the chromophores. The coordinate system *xyz*, with the *z* axis along the helical axis, defines the frame of reference for the polymers. In the side view, the chromophores pointing to the front and back have been omitted for clarity.

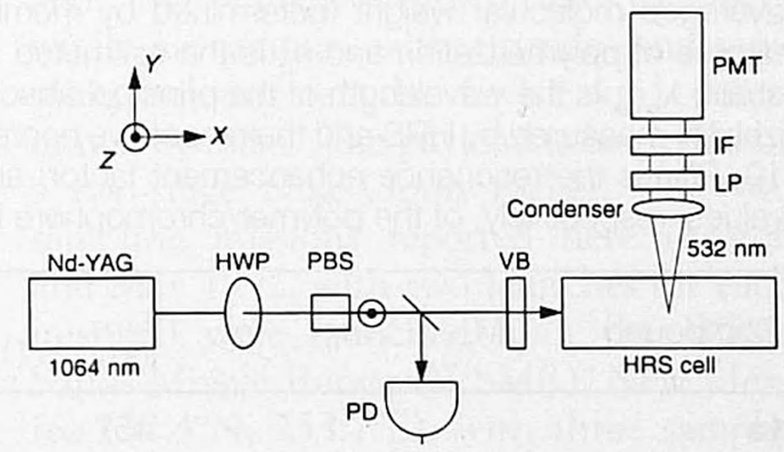

Fig. 3. HRS experimental setup. The 1064-nm output of an injection-seeded Nd–yttrium-aluminum-garnet (Nd-YAG) laser (pulse length, ~10 ns; repetition rate, 10 Hz) provides the fundamental beam to the HRS cell. The fundamental beam propagates in the positive *X* direction and is linearly polarized in the *Z* direction; unpolarized second-harmonic light at 532 nm is detected in the *Y* direction. A half-wave plate (HWP) and a polarizing beam splitter (PBS) are used to control the power of the beam. A portion of the beam is directed onto a photodiode (PD) for power monitoring. A visible blocking filter (VB) isolates the experiment from visible background light. The scattered light at 532 nm is collected with a condenser system and filtered with a low-pass filter (LP) and an interference filter (IF) before detection with a photomultiplier (PMT).

mophore. This approach is consistent with the sum-over-states method of calculating molecular hyperpolarizabilities (*1*) in the limit in which the excitations are assumed to be localized in the chromophores. In this limit, excitonic effects are neglected and the shift in the absorption spectrum of the polymers relative to that of the chromophores arises from a perturbative interaction between the chromophores (*14*).

For long conjugated chromophores, the dominant hyperpolarizability component is $\beta_{uuu} \equiv \beta_u$, where u is the long axis. For an isotropic transverse distribution of chromophores, the polymer chains belong to symmetry group $C_{\infty v}$ if the helicity of the backbone is neglected. For this symmetry group, the nonvanishing components of the hyperpolarizability tensor are zzz, $zxx = zyy$, and $xxz = xzx = yyz = yzy$, where z is the axis of the helix and x and y are the transverse coordinates. By projecting the chromophoric coordinate (u) onto the polymeric coordinates (xyz), we obtain

$$\beta_{zzz} = n_c\beta_u \cos^3\theta = 0.125 n_c\beta_u \quad (3)$$

$$\beta_{zxx} = \beta_{xxz} = \frac{1}{2} n_c\beta_u \sin^2\theta \cos\theta = 0.1875 n_c\beta_u \quad (4)$$

where n_c is the degree of polymerization (that is, the number of chromophores in a polymer chain) and θ is the angle between the helical axis and the chromophores. The numerical prefactors were obtained for $\theta = 60°$. The quantity measured in our HRS experiment that used unpolarized detection is

$$\beta^2_{solute} = \langle\beta^2_{ZZZ}\rangle + \langle\beta^2_{XZZ}\rangle \quad (5)$$

where XYZ is the laboratory frame of reference and the brackets denote orientational averaging over the isotropic distribution of the molecules (polymers or chromophores) in the scattering solution. The orientational averages were calculated with a transformation between the molecular and laboratory frames of reference (*15*). The effective hyperpolarizabilities of the polymers and chromophores measured in the HRS experiment were

$$\beta^2_{polymer} = \frac{8.53}{210} n_c^2\beta_u^2 \quad (6)$$

and

$$\beta^2_{chromophore} = \frac{36}{210}\beta_u^2 \quad (7)$$

respectively. The ratio of these quantities, which corresponds to the expected increase in the value of the hyperpolarizability, is

$$E = \frac{\beta_{polymer}}{\beta_{chromophore}} = 0.487 n_c \quad (8)$$

In Eq. 6, β_u represents the hyperpolarizability of the individual chromophores in the polymeric environment, whereas in Eq. 7, β_u represents the hyperpolarizability of the free chromophores. These two quantities are not necessarily equal. In our polymers, the properties of the chromophores are perturbed by their mutual interaction, as shown by the blue shift in the absorption spectra of the polymers. As a consequence, the hyperpolarizabilities of the polymers and chromophores are resonantly enhanced by different amounts, and it is more appropriate to compare the nonresonant values of the hyperpolarizabilities in our model. Within the two-level model of molecular nonlinearities (*1*), the resonantly enhanced hyperpolarizability can be expressed as

$$\beta(\omega) = R(\omega)\beta_0 \quad (9)$$

where β_0 is the nonresonant value and the resonance enhancement factor is

$$R(\omega) = \frac{\omega_0^4}{(\omega_0^2 - \omega^2)(\omega_0^2 - 4\omega^2)} \quad (10)$$

In Eq. 10, $\omega_0 = 2\pi c/\lambda_{max}$, where λ_{max} is the wavelength at which the maximum of the principal absorption band occurs, and ω corresponds to the wavelength of the laser. Note that the ordering of the chromophores in the polymer chain is not perfect; the ordering is expected to be poor for the first two and last two helical turns of the backbone. Hence, the number of chromophores n_c' that contribute coherently to the hyperpolarizability of the polymer chain is lower than the total number of chromophores by ~15, and Eq. 8 should be used with this fact in mind.

In the analysis of our measurements, we have included the corrections that arise from the reduced number of organized chromophores and from the resonance enhancement factor (Table 1). The theoretical model predicts a large increase in the hyperpolarizability of the polymers compared with that of the individual chromophores, and such an increase was observed experimentally. The quantitative discrepancy between the predicted and observed increase is believed to be the result of additional uncertainties in the values of the parameters of the model. These uncertainties include (i) the neglect of damping, even though the excitation is near two-photon resonant; (ii) the sensitivity of the hyperpolarizability components of the polymer to the exact value of the angle between the axis of the polymer and the chromophores; and (iii) the reduction in the peak absorbance of the polymers relative to that of the individual chromophores. Moreover, the number of chromophores that contribute coherently to the hyperpolarizability of the polymer could be lower than estimated because of delocalization of the excitations.

We next investigated the extent to which the polymers could be aligned through poling. We performed electric field–induced second-harmonic generation measurements on the chromophore **1a** and the polymer **1b**; these measurements determine the product of the permanent dipole moment and the vectorial part of the hyperpolarizability ($\mu\beta^{vec}$) of the compounds. This quantity was measured as 1120×10^{-48} esu and $131{,}000 \times 10^{-48}$ esu for individual chromophores and polymers, respectively. The corresponding nonresonant values $\mu\beta_0^{vec}$, which were calculated with the resonance enhancement factors of Table 1, were 239×10^{-48} esu and $35{,}200 \times 10^{-48}$ esu, respectively. Thus, the product $\mu\beta_0^{vec}$ of the polymers was more than two orders of magnitude greater than that of the monomers. More important, an enhancement of $\mu\beta_0^{vec}$ per chromophore (relative to individual chromophores) was observed in the polymer structure. Hence, for a fixed number of chromophore molecules, poling of the polymer structure results in a larger nonlinear response than does poling of individual chromophores. For off-resonant excitation, this enhancement factor is ~1.5.

The structures of the poly(isocyanide)s investigated were not optimized for large supramolecular effects in the second-order nonlinear response, primarily because of the large angle (~60°) between the axis of the helical backbone and the chromophores. This structure gives rise to large off-diagonal components of the hyperpolarizability tensor, which cannot be used to full advantage in the poling process. However, our results

Table 1. Properties of the individual chromophores and the poly(isocyanide)s. $\overline{M}_n$ is the number-averaged molecular weight (determined by membrane osmometry in chloroform at 34°C); n_c is the degree of polymerization and n_c' is the estimated number of well-ordered chromophores in a polymer chain; λ_{max} is the wavelength of the principal absorption maximum; β^{HRS} and β_0^{HRS} are the hyperpolarizability measured by HRS and the respective nonresonant hyperpolarizability estimated from Eqs. 9 and 10; $R(\omega)$ is the resonance enhancement factor; and E_{theor} and E_{expt} are the predicted and measured values, respectively, of the polymer/chromophore hyperpolarizability ratio.

Compound	$\overline{M}_n$	n_c	n_c'	λ_{max} (nm)	β^{HRS} (10^{-30} esu)	$R(\omega)$	β_0^{HRS} (10^{-30} esu)	E_{theor}	E_{expt}
1a	–	1	–	457	774	4.68	165	–	–
1b	51,000	97	82	438	3020	3.73	810	40	4.9
2a	–	1	–	448	564	4.18	135	–	–
2b	40,000	94	79	435	5150	3.62	1420	38	11

provide a conclusive demonstration of the principle of the enhancement of nonlinear optical response through the supramolecular engineering of polymers. It is expected that considerably larger enhancement can be observed in structures with better alignment of chromophores, such as certain biopolymers and derivatives of helical poly(triphenylmethylmethacrylate)s (*16*).

REFERENCES AND NOTES

1. See, for example, P. N. Prasad and D. J. Williams, *Introduction to Nonlinear Optical Effects in Molecules and Polymers* (Wiley, New York, 1991).
2. J.-M. Lehn, *Supramolecular Chemistry* (VCH, Weinheim, Germany, 1995).
3. K. Clays *et al., Science* **262**, 1419 (1993).
4. E. Kelderman *et al., Adv. Mater.* **5**, 925 (1993).
5. C. T. O'Konski, K. Yoshioka, W. H. Orttung, *J. Phys. Chem.* **63**, 1558 (1959).
6. R. J. M. Nolte, A. J. M. van Beijnen, W. Drenth, *J. Am. Chem. Soc.* **96**, 5932 (1974); R. J. M. Nolte, *Chem. Soc. Rev.* **23**, 11 (1994).
7. M. N. Teerenstra *et al., Thin Solid Films* **248**, 110 (1994).
8. R. J. M. Nolte and W. Drenth, in *New Methods for Polymer Synthesis*, W. J. Mijs, Ed. (Plenum, New York, 1992), pp. 273–310. For a discussion of the structure of poly(isocyanide)s, see also M. M. Green, R. A. Gross, F. C. Schilling, K. Zero, C. Crosby III, *Macromolecules* **21**, 1839 (1988); C. Kollmar and R. Hoffman, *J. Am. Chem. Soc.* **112**, 8230 (1990).
9. C. J. M. Huige, A. M. F. Hezemans, R. J. M. Nolte, W. Drenth, *Recl. Trav. Chim. Pays-Bas* **112**, 33 (1993).
10. R. W. Terhune, P. D. Maker, C. M. Savage, *Phys. Rev. Lett.* **14**, 681 (1965).
11. K. Clays and A. Persoons, *ibid.* **66**, 2980 (1991); *Rev. Sci. Instrum.* **63**, 3285 (1992).
12. T. Verbiest, E. Hendrickx, A. Persoons, K. Clays, in *Nonlinear Optical Properties of Organic Materials V*, D. J. Williams, Ed. [*Proc. SPIE* **1775**, 206 (1993)].
13. G. S'heeren, L. Derhaeg, T. Verbiest, C. Samyn, A. Persoons, *Makromol. Chem., Makromol. Symp.* **69**, 193 (1993).
14. R. S. Becker, *Theory and Interpretation of Fluorescence and Phosphorescence* (Wiley, New York, 1969), chap. 16.
15. R. Bersohn, Y.-H. Pao, H. L. Frisch, *J. Chem. Phys.* **45**, 3184 (1966).
16. T. Nakano, Y. Okamoto, K. Hatada, *J. Am. Chem. Soc.* **114**, 1318 (1992).
17. M. N. Teerenstra *et al.*, in preparation.

18. Supported by grants from the government of Belgium (IUAP-16), the Belgian National Science Foundation (FKFO 9.0011.92), and the University of Leuven (GOA95/1) (to M.K., T.V., C.B., K.C., and A.P.) and from the Dutch Ministry of Economical Affairs (IOP-PCBP 105) (to M.N.T., A.J.S., and R.J.M.N.). M.K. is a research fellow of the University of Leuven; T.V. is a postdoctoral researcher and K.C. is a senior research associate of the Belgian National Fund for Scientific Research (NFWO).

11 July 1995; accepted 11 September 1995

Carbon Dioxide and Oxygen Isotope Anomalies in the Mesosphere and Stratosphere

Mark H. Thiemens,* Teresa Jackson, Edward C. Zipf, Peter W. Erdman, Cornel van Egmond

Isotopic ($\delta^{17}O$ and $\delta^{18}O$) measurements of stratospheric and mesospheric carbon dioxide (CO_2) and oxygen (O_2), along with trace species concentrations (N_2O, CO, and CO_2), were made in samples collected from a rocket-borne cryogenic whole air sampler. A large mass-independent isotopic anomaly was observed in CO_2, which may in part derive from photochemical coupling to ozone (O_3). The data also require an additional isotopic fractionation process, which is presently unidentified. Mesospheric O_2 isotope ratios differed from those in the troposphere and stratosphere. The cause of this isotopic variation in O_2 is presently unknown. The inability to account for these observations represents a fundamental gap in the understanding of the O_2 chemistry in the stratosphere and mesosphere.

The measurement of stable isotope ratios of atmospheric species provides a powerful method for investigating chemical transformation mechanisms in the atmosphere. A particularly important example is stratospheric O_3, for which an ^{18}O enrichment of up to 40% in the $^{18}O/^{16}O$ ratio has been observed (*1–4*). In laboratory studies of isotopic fractionation during O_3 formation, O_3 was produced that was enriched in the heavy isotopes, with $\delta^{17}O = \delta^{18}O$, rather than $\delta^{17}O = 0.5\ \delta^{18}O$ (*5*, *6*). The isotope ratios were thus distributed in a mass-independent manner; in a mass-dependent process, the $\delta^{18}O$ variation would be twice that of $\delta^{17}O$ because the relative mass difference is doubled (*5*). It has been demonstrated that the anomalous fractionation occurred in the $O + O_2$ recombination step and was mediated by molecular symmetry factors (*7*). Many of the observed stratospheric O_3 ^{18}O enrichments are significantly greater than those observed in laboratory experiments, which are at most 150 per mil (*8–10*). To date, there is no consistent explanation for this large discrepancy or for the observed variability of the ^{18}O enrichment in stratospheric O_3. The inability to account for these observations represents a fundamental gap in the understanding of stratospheric O_3 chemistry.

Stratospheric CO_2 has also been shown to be enriched in ^{18}O in comparison with tropospheric CO_2 (*11–13*), and it has been shown that stratospheric O_2 isotopes are mass-fractionated independently (*12*). It has been proposed that the CO_2 enrichment may arise from isotopic exchange between CO_2 and $O(^1D)$, with $O(^1D)$ derived from O_3 photolysis (*14*). Laboratory experiments demonstrated that isotopic exchange between $O(^1D)$ and CO_2 produces a mass-independent fractionation, with equal enrichment in the heavy isotopes in CO_2 (*15*). Recent simultaneous $\delta^{17}O$ and $\delta^{18}O$ measurements of stratospheric CO_2 have demonstrated that the magnitude of the mass-independent isotopic anomaly linearly correlates with ^{14}CO activity, which confirms the stratospheric origin of the isotopic enrichment (*13*). The use of simultaneous isotope ratio measurements ($\delta^{17}O$ and $\delta^{18}O$) thus offers an insight into atmospheric chemical processes that cannot be obtained from concentration or measurements of single ($\delta^{18}O$) isotope ratios.

The observation of photochemical coupling between stratospheric O_3 and CO_2 has several implications. First, the CO_2 isotopic measurements provide another probe of the overall oxidation processes of the upper atmosphere (*13*). In particular, estimates of the $O(^1D)$ density can be obtained, which determines the lifetime of some of the more long-lived species, such as N_2O, and is an integral component of the radiative budget of the upper atmosphere. Second, the O_2 isotopes provide another measure of stratosphere-troposphere mixing.

Here, we report the simultaneous measurement of the $\delta^{17}O$ and $\delta^{18}O$ composition of CO_2 and O_2 and the concentrations of N_2O, CH_4, and CO from samples taken in the altitude range of 30 to 60 km. Samples were taken with the use of the rocket-borne cryogenic whole air sampler (CWAS) described by Erdman and Zipf (*16*). The system uses closed-cycle refrigerators to chill 1.8-kg, gold-plated blocks to approximately 15 K. Pneumatically actuated valves open and close at predetermined times to collect whole air samples, with altitudes and sampling column lengths (~1.1 km) determined by radar. The payload is launched by a two-stage Nike-Orion rocket. The two sampling missions reported here (March and May 1992, with two launches for each mission) were launched from the White Sands Missile Range (WSMR), New Mexico (32.4°N, 253.7°E), with three samples collected per flight (Table 1). The altitudes of the samples, the sampling interval, and the absolute sample sizes were nearly iden-

M. H. Thiemens and T. Jackson, Department of Chemistry 0356, University of California at San Diego, La Jolla, CA 92093, USA.
E. C. Zipf, P. W. Erdman, C. van Egmond, Department of Physics and Astronomy, University of Pittsburgh, Pittsburgh, PA 15260, USA.
*To whom correspondence should be addressed.